# THE *KEPLER* DICHOTOMY IN PLANETARY DISKS: LINKING *KEPLER* OBSERVABLES TO SIMULATIONS OF LATE-STAGE PLANET FORMATION

John Moriarty[1] and Sarah Ballard[2]
[1] Yale University, New Haven, CT 06511, USA; john.c.moriarty@yale.edu
[2] Massachusetts Institute of Technology, Cambridge, MA 02139 USA

## ABSTRACT

NASA's *Kepler* Mission uncovered a wealth of planetary systems, many with planets on short-period orbits. These short-period systems reside around 50% of Sun-like stars and are similarly prevalent around M dwarfs. Their formation and subsequent evolution is the subject of active debate. In this paper, we simulate late-stage, in situ planet formation across a grid of planetesimal disks with varying surface density profiles and total mass. We compare simulation results with observable characteristics of the *Kepler* sample. We identify mixture models with different primordial planetesimal disk properties that self-consistently recover the multiplicity, radius, period and period ratio, and duration ratio distributions of the *Kepler* planets. We draw three main conclusions. (1) We favor a "frozen-in" narrative for systems of short-period planets, in which they are stable over long timescales, as opposed to metastable. (2) The "*Kepler* dichotomy," an observed phenomenon of the *Kepler* sample wherein the architectures of planetary systems appear to either vary significantly or have multiple modes, can naturally be explained by formation within planetesimal disks with varying surface density profiles. Finally, (3) we quantify the nature of the "*Kepler* dichotomy" for both GK stars and M dwarfs, and find that it varies with stellar type. While the mode of planet formation that accounts for high multiplicity systems occurs in 24% ± 7% of planetary systems orbiting GK stars, it occurs in 63% ± 16% of planetary systems orbiting M dwarfs.

*Key words:* planets and satellites: formation

## 1. INTRODUCTION

One of the most important findings of NASA's *Kepler* mission is the prevalence of planets on relatively short-period orbits. M dwarfs host, on average, 2.5 planets per star, with radii between 1 and $4R_\oplus$ and orbital periods shorter than 200 days (Morton & Swift 2014; Dressing & Charbonneau 2015) and nearly half of all G and K stars host at least 1 planet within the same range (Petigura et al. 2013; Silburt et al. 2015). The ubiquity of these planetary systems has sparked a number of investigations of their underlying architecture. The most straightforward observable to compare with predictions is the number of transiting planets ("tranets") per system. Constructing a set of synthetic planetary systems and then "observing" them from random angles provide a means of comparison to the *Kepler* tranet yield. These studies constrain the underlying multiplicity of the systems and distribution of planet inclinations. The general consensus from these simulations is that planetary systems tend to be very flat (mutual inclinations less than a few degrees) (Fang & Margot 2012; Figueira et al. 2012; Swift et al. 2013; Ballard & Johnson 2014; Fabrycky et al. 2014).

However, there exists a strong degeneracy between the underlying multiplicity and the mutual inclinations of the planets. That is, systems with more planets with higher mutual inclinations will present the same number of transiting planets as systems with fewer planets with lower mutual inclinations. Transit duration ratios of adjacent planets, which are sensitive to the inclination distribution of planets, provide a means to break this degeneracy. Both Fang & Margot (2012) and Fabrycky et al. (2014) folded transit duration ratios into their analyses and concluded that most systems have one to two planets with mutual inclinations between planets less than 3°.

Other studies have found that the observed population of planets is not well described by a single-component model of system architecture. Lissauer et al. (2011) and Ballard & Johnson (2014) both find that their best-fitting single-component models significantly underpredict the number of singly transiting systems. Hansen & Murray (2013) compare planetary systems created in late-stage planet formation simulations to observed systems and similarly find that singly transiting systems are 50% more common in the observed population than their modeled population. Looking beyond multiplicity, Xie et al. (2014) compared the fraction of transiting planets showing transit timing variations (TTVs) for single versus multi-planet systems and found that systems with four or more transiting planets show TTVs at a rate ~5 times higher than those of singly transiting systems. These findings all suggest that the underlying architecture of planetary systems is better described by either a mixture model or a continuum of architectures.

Qualitatively, a mixture model must consist of one component with many planets on low mutual inclinations that accounts for the majority of systems with two or more transiting planets. The other component must account for the majority of systems with only one transiting planet. These latter systems either host fewer planets, or their planets possess high mutual inclinations so that only one planet will transit from any given viewing angle. The utility of transit duration ratios as a tool for probing mutual inclination is lost for systems with only one transit. Morton & Winn (2014) find that the stellar obliquity of systems with only one transiting planet is systematically higher than for systems with multiple transiting planets. This may suggest that the second population is made up of planets with high mutual inclinations. However, it is possible that whichever potential mechanism reduces the underlying multiplicity of systems also increases obliquity.

A number of authors have explored the possibility that a dichotomy in the structure of planetary systems can arise from

the long-term evolution of dynamically full systems. Volk & Gladman (2015) suggest that systems of many tightly packed planets are the normal outcome of planet formation and that some fraction of these systems eventually undergo a dynamical instability which leads to the consolidation of these systems into fewer planets. Similarly, Pu & Wu (2015) find that many of the *Kepler* multi-planet systems are metastable. They propose that the lower multiplicity systems are resultant from more densely packed systems that have undergone a period of dynamical instability. On the other hand, Johansen et al. (2012) find that dynamical instability is probably not the cause of the *Kepler* dichotomy. They followed the evolution of triple systems with the goal of producing doubles with high mutual inclinations. However, they found that the timescales needed for instability to occur are very long unless the planets are very high mass. Planets of 0.1–10 Jupiter masses are needed for instability to occur within 10 billion years. Similarly Becker & Adams (2015) found that self-excitation is rarely sufficient to remove planets from the transiting geometry.

We explore this hypothesis through *N*-body simulations of late-stage planet formation and a comparison of these simulations results in the observed population of planets. We investigate whether two properties, (1) the total mass of planetesimals within the protoplanetary disk and (2) the radial distribution of this mass, determine the final multiplicity of planetary systems and the mutual orbital inclinations of the planets. In Section 2, we describe the details of our simulations, and in Section 3 describe their results. In Section 4, we compare observable quantities from our simulations—number of transiting planets, transit duration ratio, and period ratio—to *Kepler* observations. In Section 5, we describe the application of our simulations specifically to the sample of planets orbiting M dwarfs (Section 5.1). We go on to comment upon the possible physical origin of the variation in the properties of planetesimal disks (Section 5.2) and the long-term evolution of planetary systems (Section 5.3). In Section 5.4, we summarize the predictions from our simulations and implications for future study, and conclude in Section 6.

## 2. SIMULATIONS

The formation pathway of short-period planets is a matter of debate. Models of their formation fall into two general categories: those where planets form in situ from a massive planetesimal disk (e.g., Hansen & Murray 2012; Chiang & Laughlin 2013) and those where planets form at larger distances from the star and later migrate to their currently observed locations (e.g., Terquem & Papaloizou 2007; Cossou et al. 2014). Currently, comparison with known planetary systems does not definitively favor one model over the other. Although both models are able to form systems that generally match the architectures of observed planetary systems, neither of them have yet been able to duplicate all of their characteristics. It is expected that bodies larger than about the mass of Mars should feel significant torques from the disk (Ward 1997; Tanaka et al. 2002), enough for substantial migration over the lifetime of a protoplanetary disk. On the other hand, a strong dependence on the detailed physical structure of the disk leads to uncertainties in the magnitude and even direction of migration (Terquem 2003; Laughlin et al. 2004; Johnson et al. 2006; Masset et al. 2006; Paardekooper & Mellema 2006; Kretke & Lin 2012) indicating that we may not yet know enough about planet migration to

definitively conclude that it is important for the formation of close-in planets. In this work, we assume that planets form in situ from a previously assembled planetesimal disk.

In order to evaluate this hypothesis, we ran a large set of *N*-body simulations of late-stage planet formation. We varied both the total mass of the planetesimal disk and the radial distribution of this mass. The initial surface density of the planetesimal disk is assumed to follow a power law:

$$\Sigma = \Sigma_0 r^{\alpha}. \quad (1)$$

We choose $\alpha$ to be $-2.5$, $-1.5$, or $-0.5$ and set $\Sigma_0$ so that the total mass between 0.05 and 1 au is 7, 10, 17, or 35 $M_{\oplus}$. For each combination of $\alpha$ and disk mass we ran 32 simulations with different realizations of the initial planetesimal disk.

Motivated by the results of Kokubo & Ida (2002), we break the initial planetesimal disk into two populations: larger bodies, which we refer to as planetary embryos, and smaller bodies, which we refer to as planetesimals. Each type of body cumulatively accounts for 50% of the total planetesimal disk mass. The initial masses and semimajor axes of the embryos are determined by enforcing two requirements: (1) their radial mass distribution follows the chosen surface density power-law profile (divided by two since they only account for half the mass) and (2) they are separated by about 15 mutual Hill radii. Depending on the surface density profile, this results in anywhere from 15 to 65 embryos with a range of masses (which scale with the semimajor axis as described by Equation (3)). For each embryo, we place 10 planetesimals each with a tenth of the embryo's mass randomly positioned half way between the orbits of the embryo's inner- and outer-most nearest neighbors. The initial orbits of all bodies are close to circular ($e < 0.01$) and have low inclinations ($i < 1°$). The remaining orbital elements are assigned random values between 0° and 360°.

The evolution of each planetesimal disk around a solar-mass star was integrated using the Mercury *N*-body integrator (Chambers 1999). Collisions are assumed to result in perfect mergers of the bodies. The systems were integrated for 10 million years with a time step of 0.5 days.

## 3. RESULTS

We begin by constructing a simple model to predict the masses of planets as a function of semimajor axis given a set of initial disk conditions. In this model, the mass of a planet is determined by the size of its feeding zone and the amount of mass in that zone. We assume that the size of the feeding zone is similar to the distance between the planet and its neighbor and that this separation is some number, $\Delta$, times their mutual Hill radius,

$$r_{\rm H} \approx \left(\frac{2M_p}{3M_*}\right)^{1/3} r_p. \quad (2)$$

Given an initial power-law surface density distribution and a separation between neighboring planets, $\Delta$, the expected mass of a planet forming at a given semimajor axis is

$$M_p(r) = \frac{2(\Delta \pi \Sigma_0 r^{(\alpha+2)})^{3/2}}{\sqrt{3M_*}}. \quad (3)$$

Figure 3 shows the expected range of planetary masses (shaded in gray) assuming $15 < \Delta < 30$ (values typical for planetary systems formed in *N*-body simulations) for each
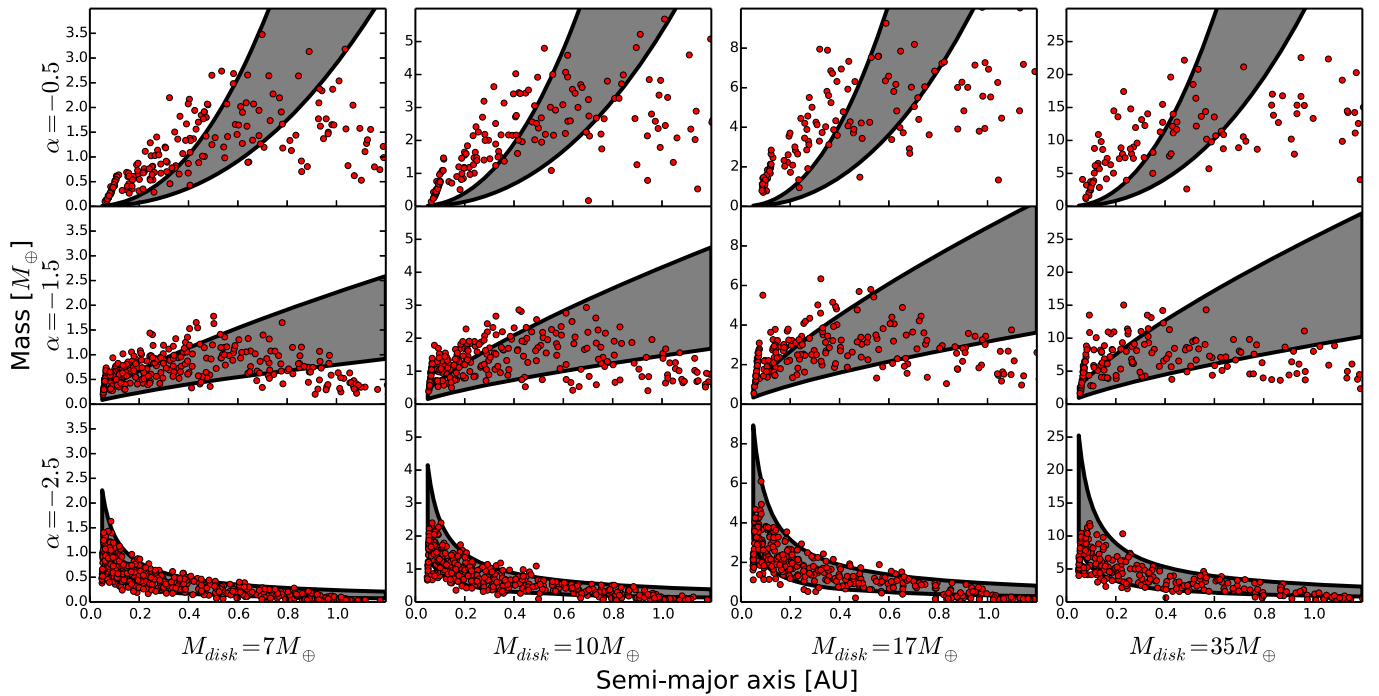
**Figure 1.** Masses and semimajor axes of the planets produced in simulations. The gray shading indicates a first-order approximation of their expected mass based on a naive model in which a planet accretes all material within its feeding zone. Deviations from this model are the result of the complex dynamics present in *N*-body simulations.

different initial planetesimal surface density distribution compared to the actual mass of planets that formed in the simulations. For $\alpha = -2.5$, this simplistic model predicts, reasonably well, the masses of planets. For larger $\alpha$, the model is a poor predictor of planet mass. The failure of this model is not surprising considering that it ignores the complex dynamical interactions present in these systems. Here, we highlight two factors that influence the mass and spacing of planets: the radial redistribution of mass and the orbital eccentricity.

Equation (3) is only valid if the final mass surface density distribution is the same as the initial one used to derive the equation. However, the numerous gravitational scatterings and resonant interactions that occur in the *N*-body simulations can significantly redistribute mass in the system. Figure 2 shows the averaged surface density distributions of the final planetary systems relative to the initial planetesimal surface density distributions. It is evident that there is some amount of mass redistribution in all systems. In particular, the outer disk, beyond ~0.6 au, loses mass during the simulation. Some of this mass is scattered outward and to conserve energy some must move inward. The inward movement of material is more apparent in the shallower surface density profile disks because there is less mass in the inner disk to begin with and any addition to this is more noticeable. This decrease of mass in the outer disk is reflected in Figure 1 in which the simulated planets are undermassive compared to what is expected from Equation (3).

The eccentricity affects the final mass of a planet because it changes the width of that planet's feeding zone. A planet on an eccentric orbit will occupy a larger radial range of the disk than one on a circular orbit. This effectively increases the value of $\Delta$ in Equation (3), leading to a larger expected mass. This effect can be seen in Figures 3 and 4. For $\alpha = -1.5$ and $-0.5$, in the

inner disk there is a rise in eccentricity and a corresponding rise in the orbital separations between neighboring planets. Thus we would expect for this region that the masses of planets that form in the simulations are larger than our simple prediction from Equation (3). Indeed, this is what we see in Figure 1.

We can start to understand the trends in eccentricity and planet–planet separations with semimajor axis by considering the angular momentum of these systems, or alternatively, the angular momentum deficit (AMD). The AMD is the difference in angular momentum that a planetary system has compared to what it would have if the orbits were circular and coplanar:

$$\text{AMD} = \sum_{k=1}^{N} \Lambda_k (1 - \sqrt{1 - e_k^2} \cos(i_k)), \qquad (4)$$

where $\Lambda_k = \frac{m_k M_\odot}{m_k + M_\odot} \sqrt{G(m_k + M_\odot)a_k}$ is the circular angular momentum of the $k$th planet. The AMD of a system provides some measure of its stability. A system with zero AMD (composed of coplanar and circular orbits) will remain stable forever, whereas a system with sufficiently high AMD will exhibit secular chaos (Wu & Lithwick 2011). Secular chaos enables the transfer of AMD between planets, leading to potentially large values of their eccentricity and inclination. Because AMD is conserved in secularly interacting systems, the maximum eccentricity a planet can attain can be calculated from Equation (4) by assuming the planet accounts for the entirety of the AMD for the system (i.e., the other planets are on circular and coplanar orbits). This is not the case for systems with resonant interactions, as in many of our simulations. However, the AMD varies by no more than a factor of a few after the first million years for most of our simulations and so the maximum eccentricity calculation is still approximately true. Figure 5 shows the maximum eccentricity calculated for
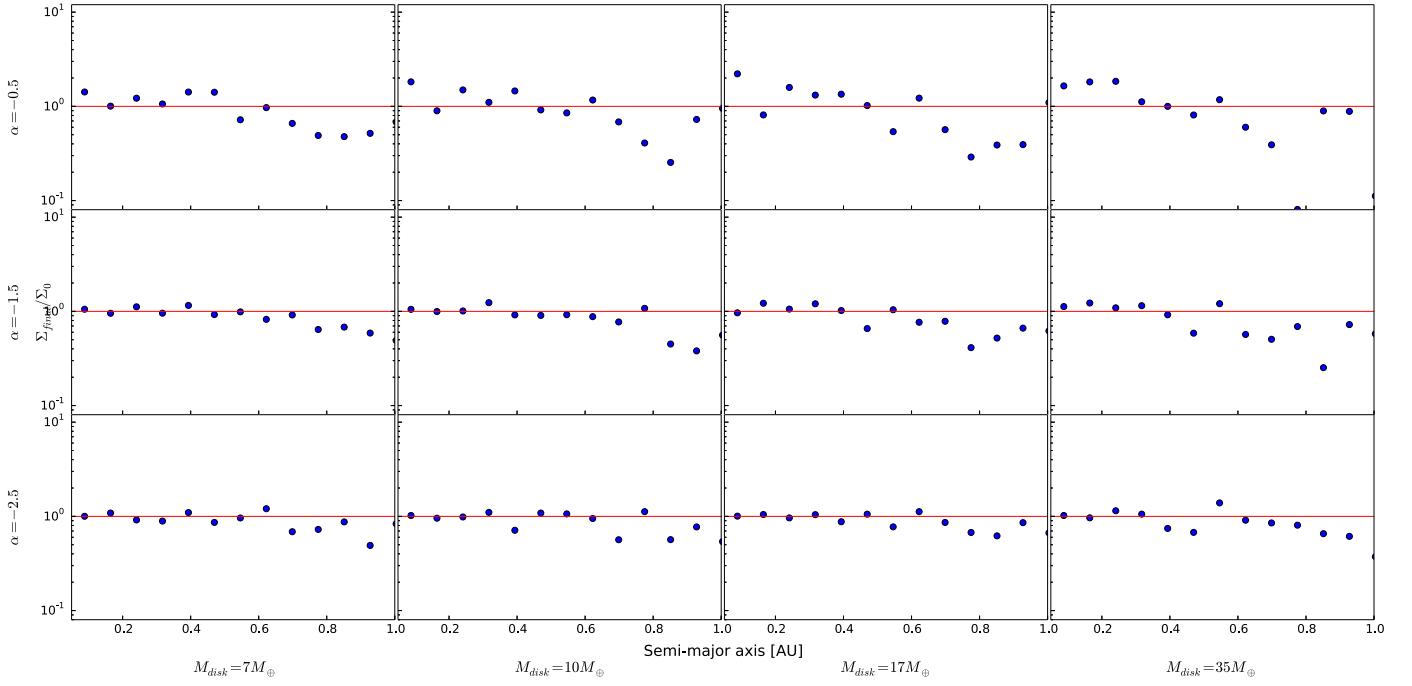
**Figure 2.** Average final surface density of simulated planetary systems divided by the initial surface density of the planetesimal disk as a function of semimajor axis. The final systems tend to be undermassive beyond about 0.6 au compared to the initial planetesimal disk as a consequence of the redistribution of mass from planetesimal–planetesimal scattering.
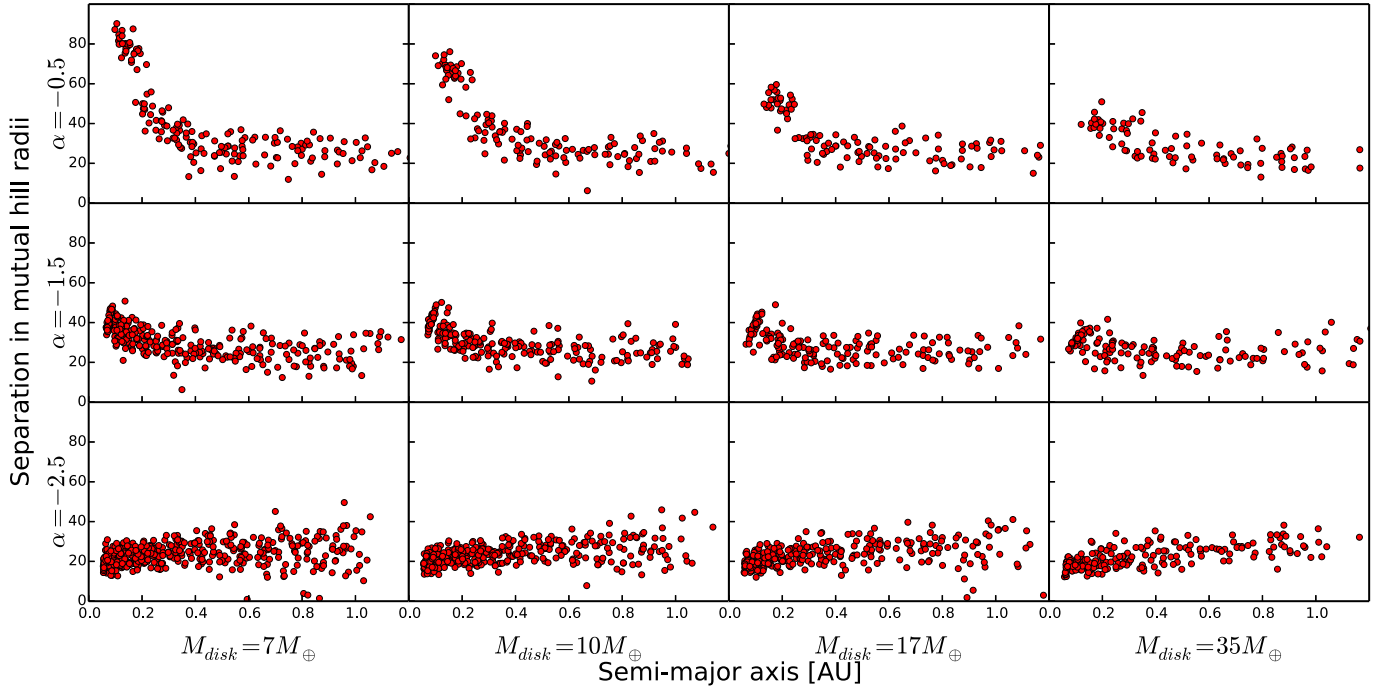


**Figure 3.** Separation between adjacent planet pairs produced in simulations in units of mutual Hill radii. Planets that form in disks with a shallower surface density profile tend to be more widely separated at smaller semimajor axes. Presumably this is due to their larger eccentricities.

each of our simulated planets given the AMD, masses, and semimajor axes of the planets at the end of the simulation. The same general trends of eccentricity with semimajor axis and initial planetesimal disk structure are apparent in the calculated maximum eccentricities and the actual eccentricities, albeit with an offset in eccentricity, indicating that secular chaos is a likely cause for the trends in eccentricity. For the simulations

with $\alpha = -0.5, -1.5$, planet mass increases with semimajor axis. Accordingly, the angular momentum of the inner planets is much smaller than that of the outer planets. In this case, a moderate fraction of the total AMD of the system can be large compared to the angular momentum of one of the inner planets. Thus if this AMD is transferred to that planet, its eccentricity can become quite large. On the other hand, in the simulations
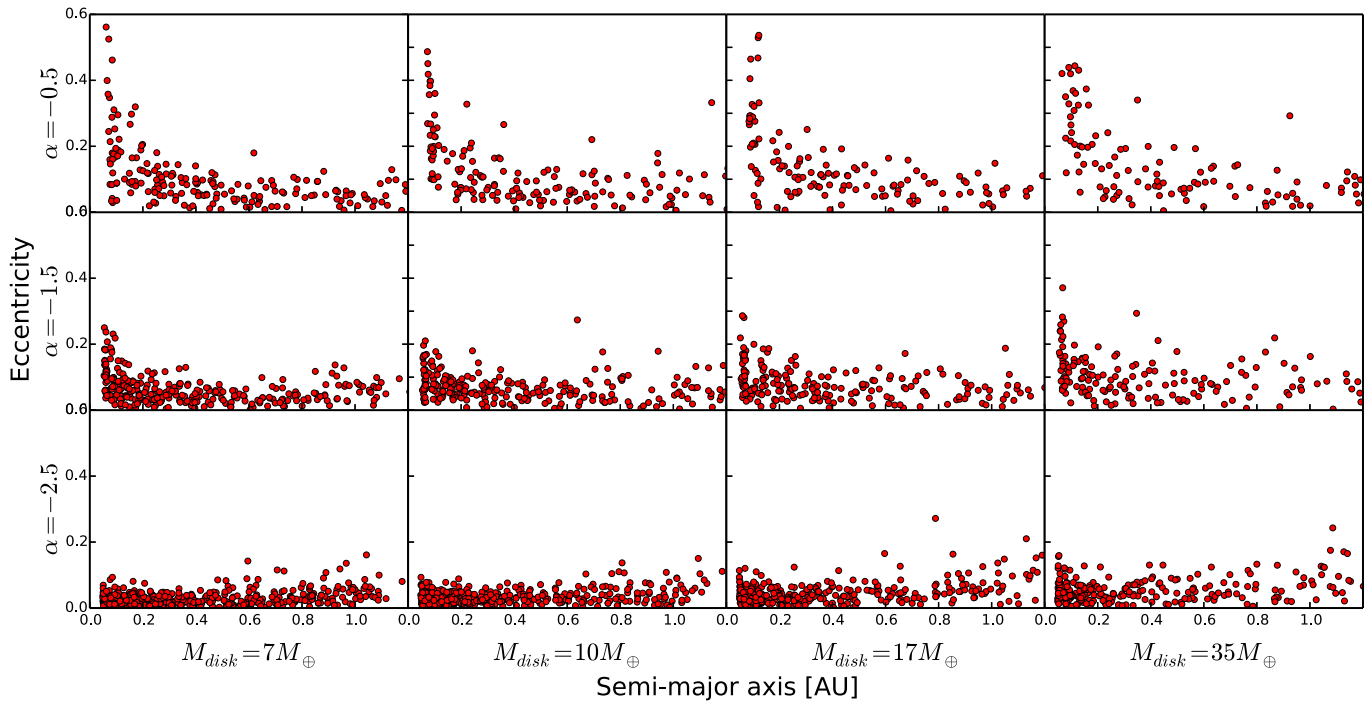
**Figure 4.** Orbital eccentricities as a function of semimajor axis for planets produced in the simulations. There is a significant rise in eccentricity at smaller semimajor axes and an overall increase in eccentricity for planets that form from planetesimal disks with shallower surface density profiles.
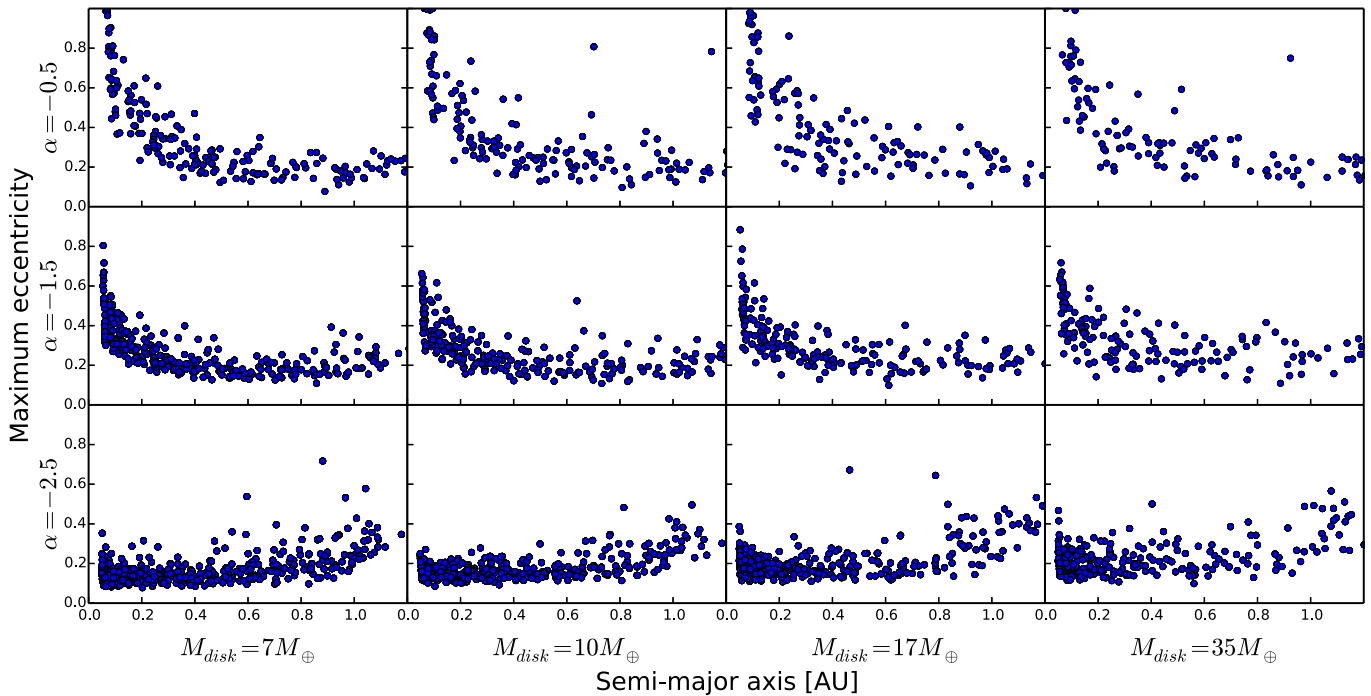


**Figure 5.** Maximum eccentricity of each simulated planet assuming all the AMD of that system is deposited on that planet. The same general trend of eccentricity with semimajor axis is seen in the maximum eccentricities as in the actual eccentricities, suggesting that secular chaos plays a large part in determining the eccentricities of the planets formed in these simulations.

with $\alpha = -2.5$, masses decrease with semimajor axis. The angular momentum of individual planets in these systems are more similar and accordingly their maximum eccentricities do not vary significantly with semimajor axis.

The distribution of masses and orbital separations of planets ultimately determine the final multiplicity of the planetary systems. Given some mass budget, an increase in orbital separation and the corresponding increase in planet mass will result in fewer planets in the system. Because the systems formed in simulations with larger values of $\alpha$ form, on average, more massive and more widely separated planets, we expect their multiplicity to be lower. This is demonstrated in Figure 6. Changing the initial distribution of mass in the planetesimal disk leads to a significant change in the multiplicity of systems
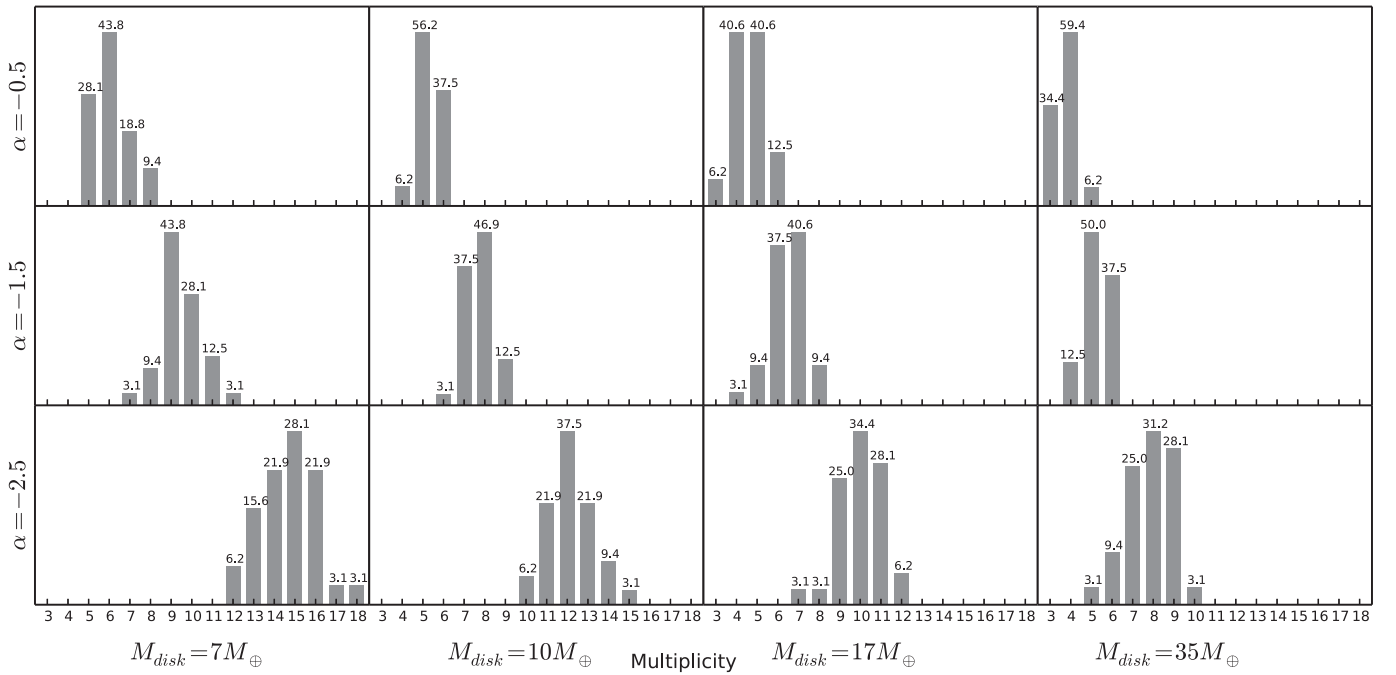
**Figure 6.** Multiplicity of systems formed with different initial planetesimal disk conditions. This includes all bodies remaining at the end of each simulation.
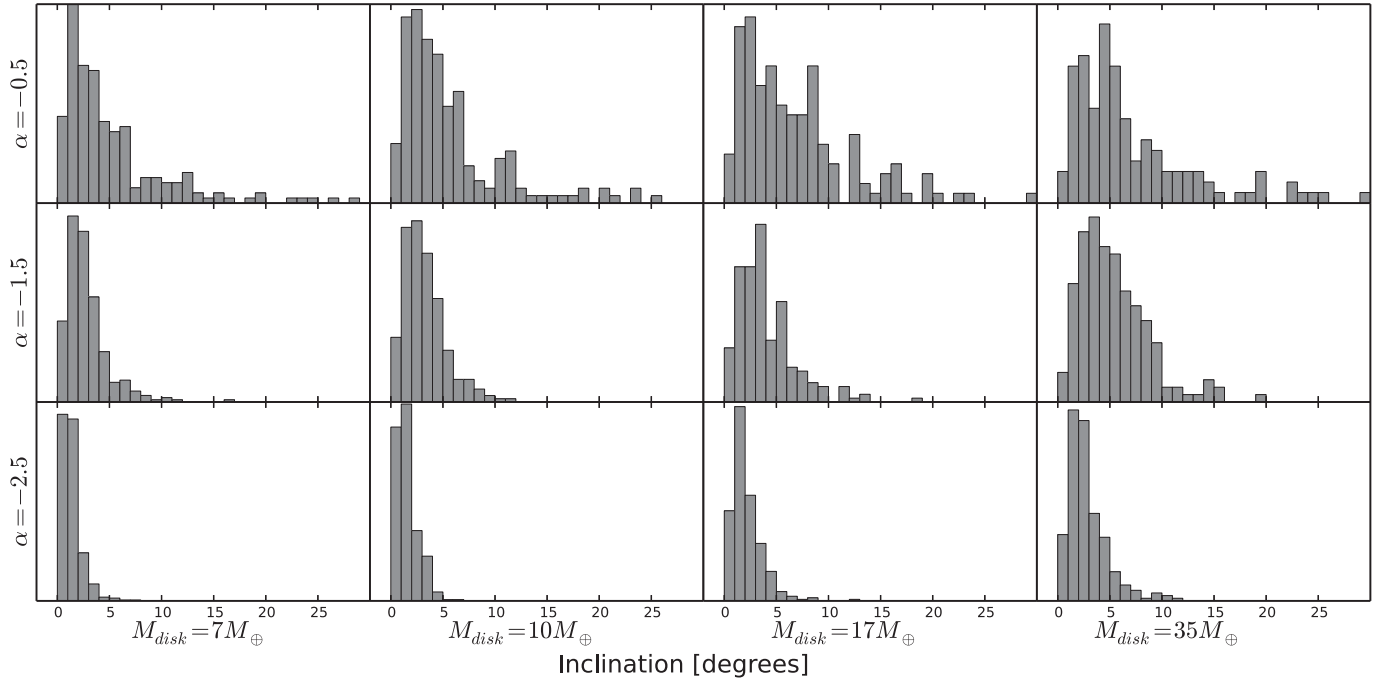


**Figure 7.** Distribution of orbital inclinations of planets formed in simulations with different initial planetesimal disk conditions.

that form. Larger $\alpha$ and higher disk mass correspond to the formation of significantly fewer planets. As we will show in Section 4, this has a strong impact on the observed multiplicity of planetary systems.

The other determining factor in the observed multiplicity of systems is the spread in mutual inclinations between planets. The effects of the initial planetesimal disk conditions on final planet inclination are significant. More massive disks tend to produce planets with moderately higher mutual inclinations and disks with larger $\alpha$ produce planets with significantly larger mutual inclinations (see Figure 7).

## 4. COMPARISON TO OBSERVATIONS

In order to compare our simulated planetary systems to the catalog of known exoplanets, we "observe" the final state of each dynamical simulation 10,000 times. We simulate the viewing geometry isotropically. Our final synthetic yield of transiting planets are those (1) with impact parameter $b < 1$ (from the given viewing angle) and (2) whose probability of detection by *Kepler* exceeds a randomly drawn uniform number between 0 and 1.

We first compare our simulations to observations of *Kepler* transiting planets orbiting GK stars. To create a realistic
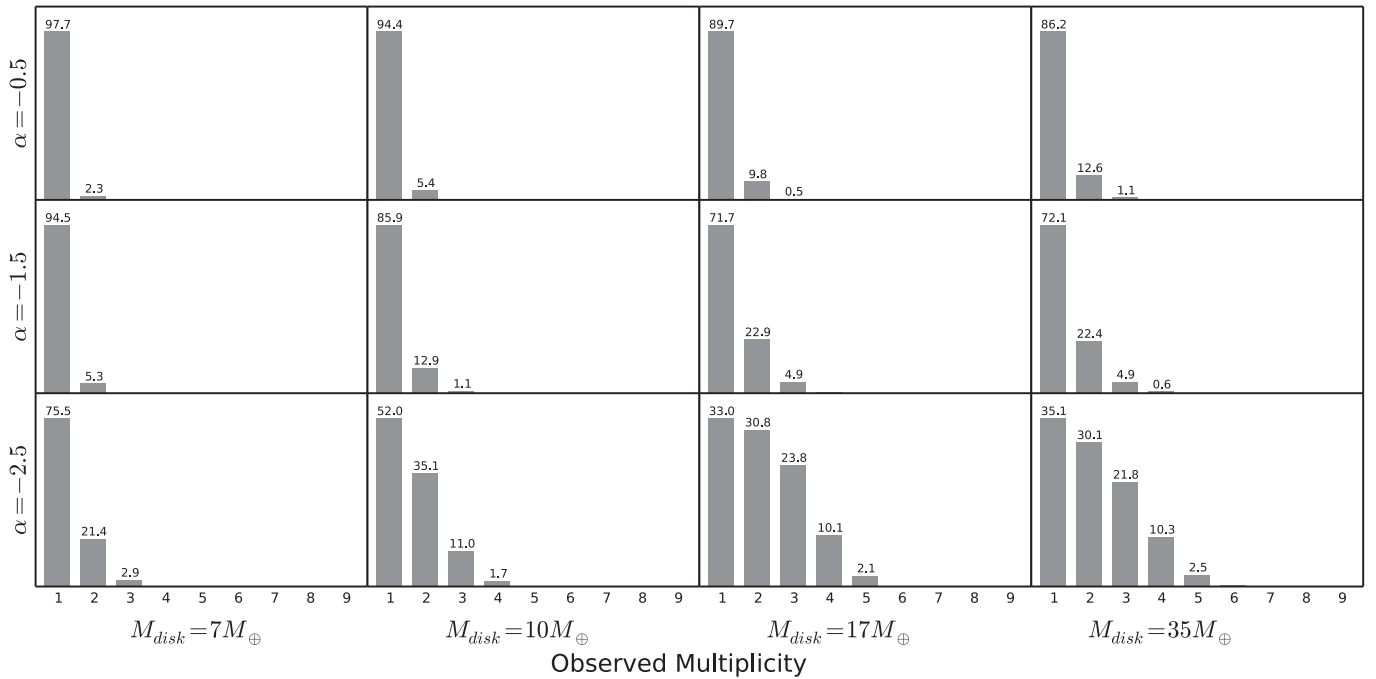
**Figure 8.** Multiplicity distribution of the simulated systems that would be observed by *Kepler*.

synthetic sample to compare to the observed sample of transiting planets, we employ the *Kepler* pipeline completeness calculation. Burke et al. (2015) contain a likelihood of detection as a function of orbital period and planetary radius. This model uses the completeness parameterization presented in Christiansen et al. (2015), itself generated from signal injection and recovery in *Kepler* data. Because our simulations calculate planet mass, we translate the planetary masses to radii to determine a detection probability for each planet. We use the probabilistic relationship presented in Wolfgang et al. (2015) for $M_p > 2.13\,M_\oplus$ (corresponding to $R_p > 1.2\,R_\oplus$, with the restriction that the radius must be greater than 1.2 $R_\oplus$. For planets with masses less than 2.13 $M_\oplus$, we use the best-fit deterministic model from Wolfgang et al. (2015) because the data do not rule out a deterministic mass–radius relation for small planets, and the scatter in the probabilistic model is unphysical for small planets. Our comparison sample consists of all known planets orbiting the stars used to calculate the detection probability grid. This sample is made up of 2,653 planets in 2042 systems.

### 4.1. Multiplicity Distribution

Figure 8 shows the distribution of apparent multiplicities from our set of "observed" systems for each initial disk structure. There is a clear dependence of the observed multiplicity on the initial planetesimal disk distribution, showing variations with both the surface density power-law index, $\alpha$, and the total initial mass in the disk, $M_{\rm tot}$.

Our observed data set $\{D\}$ is a vector with six entries, corresponding to the number of stars hosting $n$ tranets, where $1 < n < 6$. In our final *Kepler* sample, there are 1398 G and K dwarfs hosting 1 detected transiting planet, 253 hosting 2, 84 hosting 3, 37 hosting 4, 10 hosting 5, and 1 hosting 6.

We compare the model-predicted population, $\mu_n$ (with results shown in Figure 8), to the observed yield $D_n$ of tranets. We estimate the likelihood of the model we have generated

from our simulations, $\mu_n$, given $D_n$, assuming the number of systems with $n$ transiting planets is described by Poisson counting statistics. Therefore, we can describe the likelihood of the model as

$$\mathcal{L} \propto \prod_n \frac{\mu_n^{D_n} e^{-\mu_n}}{D_n!}, \qquad (5)$$

where $\mu \equiv \mu(\alpha, M_{\rm tot})$ from our dynamical simulations, and $n$ runs from 1 to 6.

We first evaluate $\mathcal{L}$ using only one mode of planet formation: that is, assuming one value for $\alpha$ and $M_{\rm tot}$. Our grid of $\alpha$ and $M_{\rm tot}$ consists of 12 points, with 3 possible values of $\alpha$ (−0.5, −1.5, and −2.5) and 4 possible values of $M_{\rm tot}$ (7, 10, 17, 35 $M_\oplus$). The model distribution, $\mu_n$, is created by re-normalizing the simulated multiplicity distribution (shown in Figure 8) to the number of systems in our observed sample. We also employ a mixture model (McLachlan & Peel 2004) to test whether the data support a model with a range of initial conditions for planet formation. We assume the simplest case of two modes, each with independent $\alpha$ and $M_{\rm tot}$, occurring with respective frequency $f$ and $(1 - f)$. The model distribution, $\mu_n$, is the weighted sum of the multiplicity distributions of each mode. We employ a uniform prior on both $\alpha$ and $M_{\rm tot}$, and employ the Bayesian sampler MultiNest (Feroz & Hobson 2008; Feroz et al. 2009, 2013) to evaluate the posterior distributions.

In agreement with previous studies, we find that the data favor a two-component model over a single-component model. Taking the ratio of the Bayesian evidences returned by MultiNest, we find a log evidence for a mixture model of −8.8, and a log evidence of −26.7 for a single mode model. We conclude that the data are better supported by a mixture model by a factor of 18:1. In Figure 9, we see that the high multiplicity tail of the multiplicity distribution requires one of the two modes to correspond to systems formed in disks with the steepest surface density profile ($\alpha = -2.5$) and a disk mass
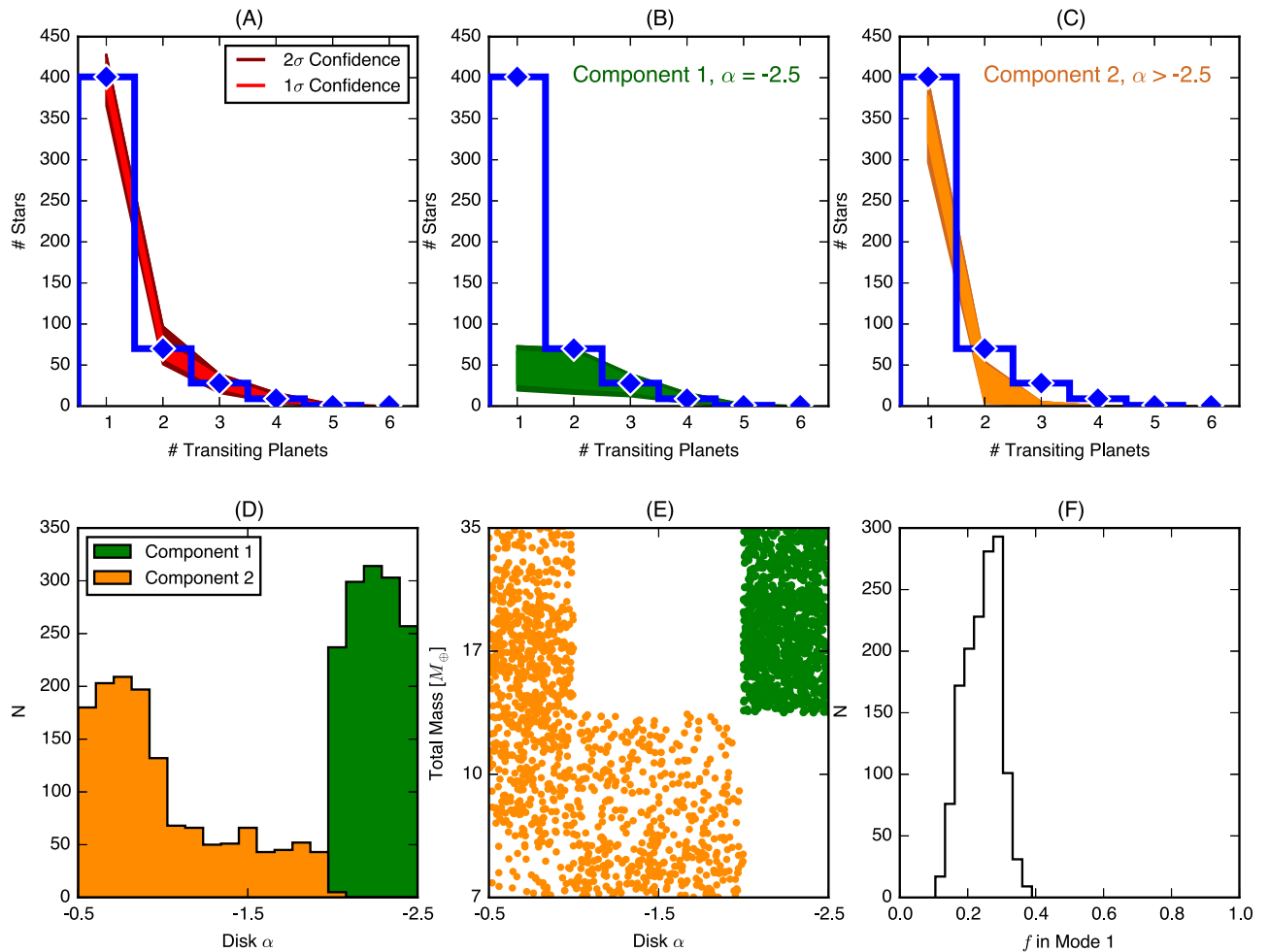
**Figure 9.** Clockwise from top left: (A) Observed distribution of tranets in blue, with the 68% and 95% (labeled as 1 and $2\sigma$) confidence model region overplotted in light and dark red, respectively. (B) $1\sigma$ region of the first component to the mixture model. (C) $1\sigma$ region of the second component to the mixture model. (D) Location of MCMC realizations in disk $\alpha$ and $M_{\rm tot}$, in green for $\{\alpha_1, M_{\rm tot,1}\}$ and orange for $\{\alpha_2, M_{\rm tot,2}\}$. (E) Marginalized posterior in $\alpha_1$ and $\alpha_2$. (F) Marginalized posterior in $f$, fraction of the mixture model in first component.

of 17 Earth-masses or greater. The mode that accounts for the high number of singly transiting systems is less well constrained because many of the disk configurations lead to systems that typically show only one transiting planet. However, models with shallower surface density profiles are favored. We find that between 15% and 35% of systems must form in the first mode while the rest form in the second.

This finding resembles that of Fang & Margot (2012), who find that 75%–80% of systems can be explained by a single description of system architecture. However, they conclude that most systems are made up of one to twp planets with low mutual inclinations, whereas we find that the underlying multiplicity and mutual inclinations are substantially larger.

The main source of error in our model is the coarseness of the simulation grid (12 sets of $\{\alpha, M_{\rm tot}\}$ in total) and the limited number (32) of simulations at each grid point. Our model error is likely larger than the uncertainties within the *Kepler* sample. Thus, it is possible that errors in our model are being over-fitted to the data. In order to ensure that our conclusions are more robust, we randomly draw a third of stars from the total set of observations $D_n$ for 10 trials. We separately evaluate the likelihood in Equation (5) for each of these smaller trial data sets, and observe whether the posterior distributions of $f$, $\alpha$, and $M_{\rm tot}$ are consistent with one another. We find that the posteriors

of $f$, $\alpha_1$, and $M_{\rm tot,1}$ are constant through these trials, with the steepest surface density profile of $\alpha_1 = -2.5$ and $M_{\rm tot} \geqslant 17\ M_\oplus$ favored. The second component to the mixture model varies, however: for some trials the data prefer the shallowest surface density profile $\alpha_2 = -0.5$ with more total mass, $M_{\rm tot,2} \geqslant 10\ M_\oplus$, and for other trials $\alpha_2 = -1.5$ is favored with less total mass. The posterior for $\{\alpha_2, M_{\rm tot,2}\}$ is very sensitive to the exact ratio of stars with two tranets to those with one tranet. We combine the posterior distributions for these 10 trials to produce the posteriors shown in in Figure 9,

### 4.2. Planet Radius and Orbital Period Distributions

Figure 10 shows the radius–period distribution of "observed" simulated planets for each set of initial disk conditions overplotted on the *Kepler* planet distribution. The predicted distribution of observed radii and orbital periods for planets that form in lower mass disks is inconsistent with the actual distribution of the *Kepler* candidates. This comparison rules them out as a primary component of the initial conditions to planet formation in our model. However, planets formed in more massive disks match the observed distribution much better.
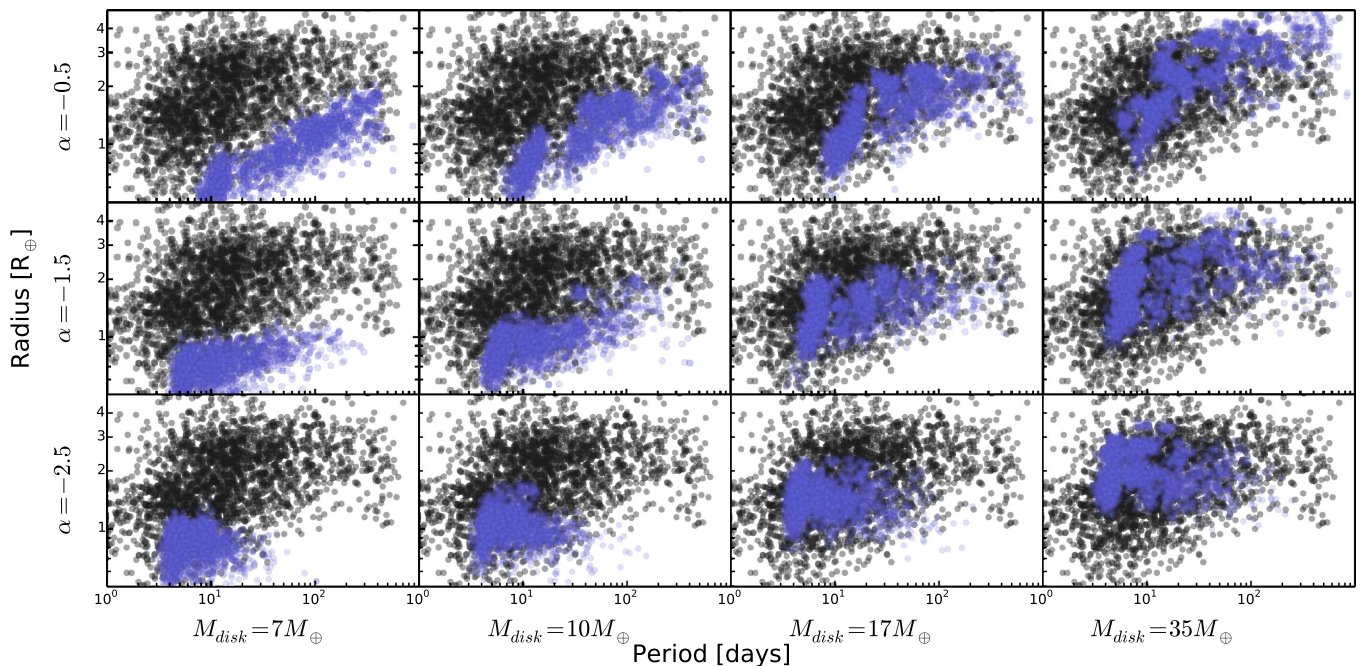
**Figure 10.** Planet radius vs. orbital period of *Kepler* candidates (gray) and "observed" simulated planets (blue) for each set of initial conditions.
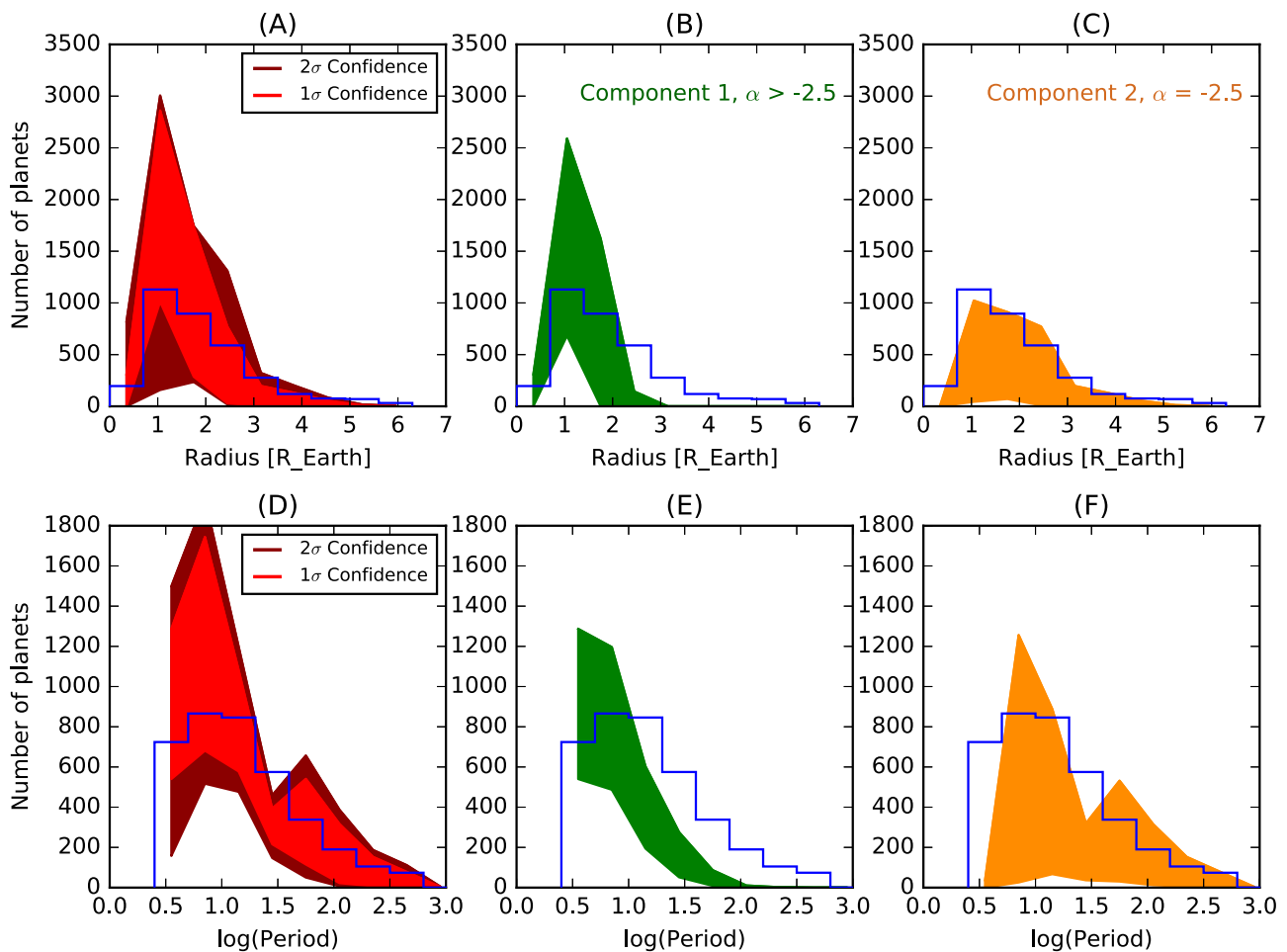


**Figure 11.** Top row: planet radius distribution of observed planets (blue histogram) compared to our modeled distribution using the mass–radius relation of Wolfgang et al. (2015). The separate model components are shown in subplots (B) and (C) and the combined fit in (A). Bottom row: same as top row but showing the distribution of orbital periods.

We note that none of the simulated planet distributions can account for the shortest period planets (<3 days). This is caused by the setup of our *N*-body simulations, which only place planetesimals between 0.05 and 1 au. Thus, it is unlikely for our simulations to form many planets within 0.05 au ($P = 4$ days). Changing the inner limit of our simulations or incorporating additional physics (e.g., tides) may solve this problem. Nevertheless, planets with periods shorter than three days account for a small fraction of the observed population and an even smaller fraction of the actual population of planets (once completeness is taken into account).

No single set of simulations is able to match the full radius–period distribution of the *Kepler* sample. Those simulations beginning with a surface density power-law index of $-1.5$ are the best match to the period distribution, but cannot simultaneously produce enough high mass (large radius) and low mass (small radius) planets. Again, this suggests that some range in the initial conditions is necessary to fit the data.

In Figure 11, we show the 1D distributions of planet radii and orbital periods of the mixture models selected from the multiplicity analysis compared to the observed distributions. In the case of orbital periods, the fit is quite good. For planet radii, the fit is good although our model does predict slightly fewer larger planets than are observed. This may suggest that some planetesimal disks are even more massive than those used in our simulations. Given that radius is not an output of our model but is derived (from planet mass), for the sake of comparison we consider the fit of the model to the data to be acceptable. We caution against any over-interpretation of the planet radii comparisons as the radii are based on an empirical mass–radius relationship that may not be valid for subsets of the modeled population. The true mass–radius relation may be a function of semimajor axis or the details of the planet assembly process (e.g., the nature and timing of the planet building collisions) as it affects gas accretion/retention. Nevertheless, on a sample-wide scale the modeled and observed distributions should be (and are) broadly consistent.

### 4.3. Duration Ratio and Period Ratio Prediction

Studies such as by Hansen & Murray (2013), Fang & Margot (2012), and Fabrycky et al. (2014) employ ensemble normalized transit durations in multi-tranet systems to infer average orbital mutual inclination.

Transit duration depends upon orbital period as well as impact parameter. The ratio of transit durations, $\xi$ (normalized by orbital velocity, per Equation (6)), of adjacent planets therefore encodes information about their mutual inclination.

$$\xi = \frac{\tau_{\mathrm{inner}}/P_{\mathrm{inner}}^{1/3}}{\tau_{\mathrm{outer}}/P_{\mathrm{outer}}^{1/3}} \qquad (6)$$

In Figure 12, we show the *Kepler* observed distribution of orbit-normalized transit durations and the *Kepler* observed distribution of period ratios for transiting planets (both in blue). We overplot our model *predictions* for these distributions that we infer from our multiplicity fit. We see that the two-component model self-consistently recovers not only the tranet distribution, but also the duration and period ratio distributions (neither of which are well-approximated by a single model).

## 5. DISCUSSION

### 5.1. Application to M Dwarf Systems

We also examine the effect of stellar mass on our simulations. There exists suggestive evidence that planet formation proceeds differently around M dwarfs than around GK dwarfs. The relationship between stellar metallicity and planet occurrence may vary as a function of stellar mass (Gaidos & Mann 2014), as well as the mass distribution of the planets themselves (Howard et al. 2012; Mulders et al. 2015). M dwarfs host, on average, 2.5 planets per star, many more than Sun-like stars (Morton & Swift 2014; Dressing & Charbonneau 2015). Intriguingly, both GK dwarfs (Lissauer et al. 2011) and M dwarfs (Ballard & Johnson 2014) also exhibit a dichotomy in their underlying architecture. For M dwarfs, a mixture model best recovers the observed multiplicity distribution. Half of these systems contain at least five planets with low mutual inclinations, and the other half containing either one planet or multiple planets with high mutual inclinations. The difference in multiplicity distribution between GK dwarfs and M dwarfs is also suggestive: one-third of M dwarfs planet hosts uncovered by *Kepler* host two or more transiting planets, while in this figure it is one in five for GK dwarfs. However, *Kepler*'s sensitivity to transits varies with stellar mass. A meaningful comparison requires folding *Kepler*'s completeness to planets into our multiplicity study.

To address this, we performed a separate set of simulations with a stellar mass of 0.5 $M_\odot$. This value corresponds to the mass of the typical M dwarf observed by *Kepler*. For this set of simulations, we began with planetesimal disks extending from 0.05–0.5 au. Rather than varying the total mass in the disk as with our GK dwarf simulations, we make the simplifying assumption that the disk contains 10 $M_\oplus$ of material. We varied the surface density profile by changing the power-law index to be $-2.5$, $-1.5$, $-0.5$, and 0.0. For each value of the power-law index we ran eight simulations.

For comparison with the *Kepler* sample, we generated synthetic "observations" in the same way we did for the solar-mass sample. We employed the detection efficiency grid for planets around M dwarfs presented in Dressing & Charbonneau (2015). We used the sample of planets detected in that work to ensure the detection efficiency was the same for the observed sample and our simulated sample. The results of the tranet fit are shown in Figure 13 and the corresponding period ratio and transit duration ratio distributions are shown in Figure 14.

We find that the data favor a mixture model by a more modest value for M dwarfs than for the GK dwarfs. A mixture model in this case returns a log evidence of $-8.4$, while a single mode model returns $-10.5$. The 2:1 evidence ratio we find in this work is less than the 8:1 stated by Ballard & Johnson (2014). We attribute this difference to the relative poorness of fit of even the mixture model in this case. Because we limited our suite of M dwarf simulations to those with a total mass of 10 $M_\oplus$, we cannot well reproduce the high tranet multiplicity that we observe. Within our GK simulations, we found that we required total masses of 17 $M_\oplus$ to recover the shape of the multiplicity distribution. We infer that increasing the available mass in our set of M dwarf simulations would similarly result in a better fit to observations.

The fractions *f* of M dwarf planetary systems that reside in the flatter geometry is 63% ± 16%, versus the 24% ± 7% of GK planetary systems. This value is consistent with the value
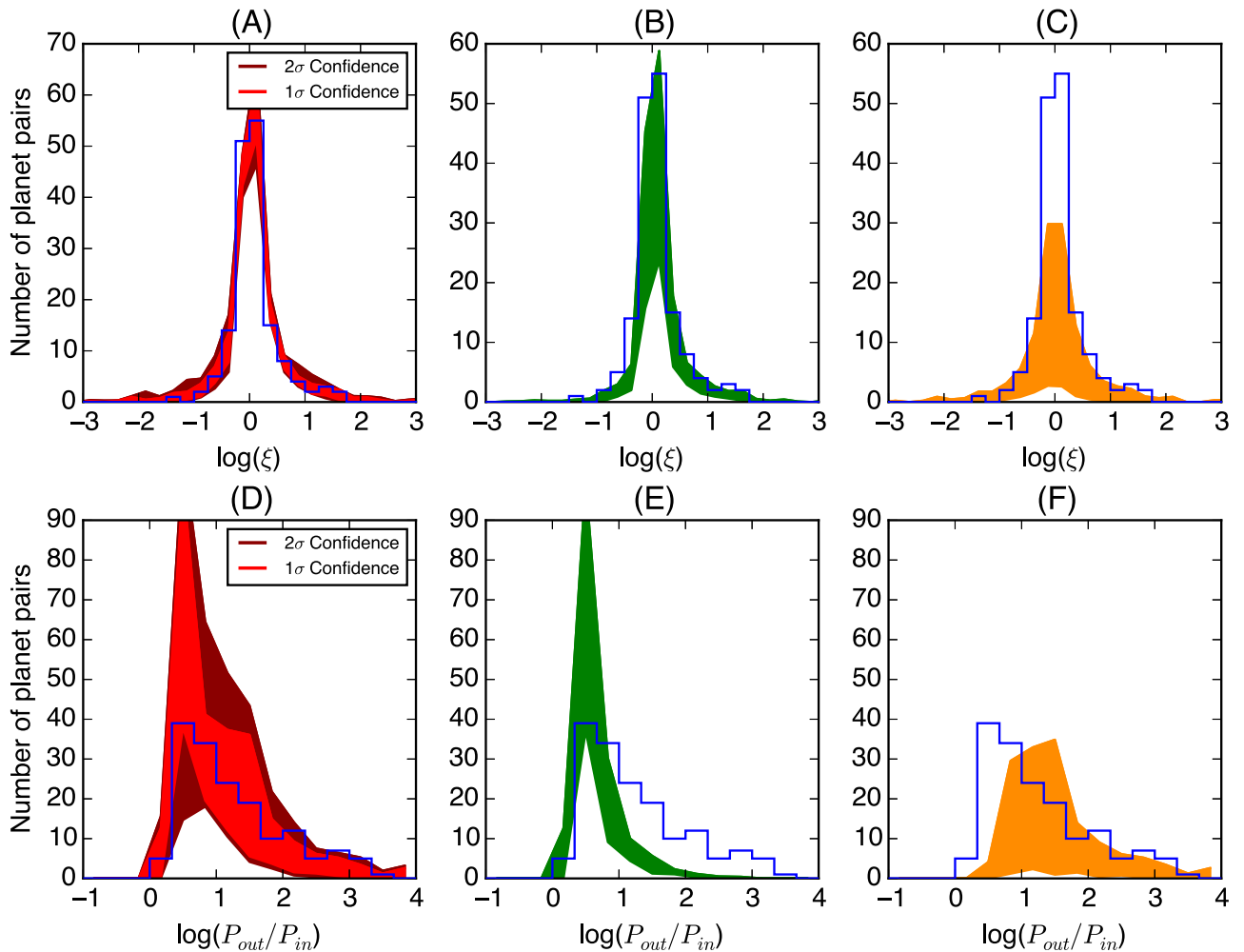
**Figure 12.** Predictions for period and duration ratio distributions, inferred from tranet fits for GK dwarfs. Clockwise from top left: (A) Observed distribution of the log of duration ratio, $\log(\xi)$, in blue. $1\sigma$ and $2\sigma$ confidence model regions are overplotted in light and dark red, respectively. (B) $1\sigma$ region of the first component to the mixture model. (C) $1\sigma$ region of the second component to the mixture model. (D) Observed distribution of $\log(P_{out}/P_{in})$ in blue, with the $1\sigma$ and $2\sigma$ confidence model regions overplotted in light and dark red, respectively. (E) $1\sigma$ region of the first component to the mixture model. (F) $1\sigma$ region of the second component to the mixture model.

of $f$ from Ballard & Johnson (2014) for M dwarf planetary systems of 47% ± 10%. The hypothesis of two distinct values for $f$ is favored by 611:1, as compared to the hypothesis that these posteriors are drawn from the same underlying distribution. We conclude that there is strong evidence for a different mixture of primordial disks around GK stars than around M dwarfs.

### 5.2. Origin of Planetesimal Disk Variation

Direct observational constraints on the distribution of mass in planetesimal disks are lacking. Estimates of planetesimal disk structure can be made by comparison to the mass profile of dust and gas disks (e.g., Raymond & Cossou 2014) or planetary systems (e.g., Weidenschilling 1977; Chiang & Laughlin 2013). However, neither the dust and gas disks nor the final systems that form from them necessarily have the same surface density profile as their planetesimal disk. Planetesimal disks form within the gas/dust disk, but they are not coupled to its viscous evolution. Consequently, the evolution of their structure is distinct. Once the planetesimal disk forms, the final planetary system is built through the scattering and merger of planetesimals. These scattering events

can lead to a significant redistribution of mass in the system, thus erasing any direct connection between the surface density profiles of the initial and final states.

The structure of planetesimal disks can also be approached from a modeling standpoint. Moriarty & Fischer (2015) simulated the growth of planetesimal disks from the accretion of inward drifting pebbles. They found that variations in the mass of the protoplanetary disk, disk metallicity, or the duration of accretion lead to planetesimal disks with different masses and radial profiles. Thus, the range of initial planetesimal disk structures required for this work may be a natural consequence of the expected variation among protoplanetary disks.

### 5.3. Long-term Evolution

The growth of planetesimal disks into planetary systems is a relatively fast process in the inner disk. Most of the evolution of these systems occurs within the first million years with collision rates dropping off significantly after that. That is not to say that longer-term evolution of these systems is not important in determining the final state of planetary systems. Other works (e.g., Pu & Wu 2015; Volk & Gladman 2015)
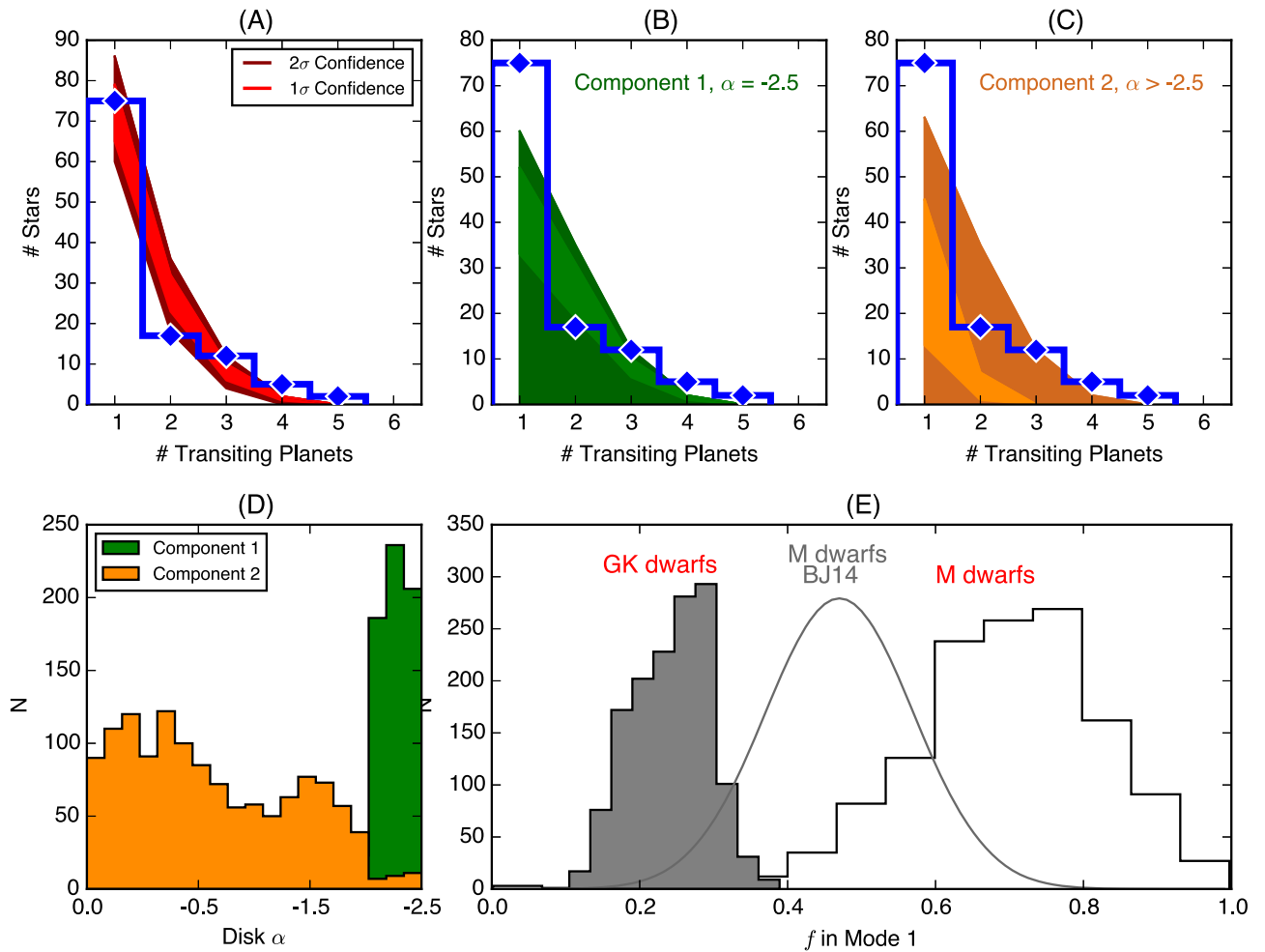
**Figure 13.** Clockwise from top left: (A) Observed distribution of tranets in M dwarf systems in blue. $1\sigma$ and $2\sigma$ confidence model regions are overplotted in light and dark red, respectively. (B) $1\sigma$ region of the first component to the mixture model. (C) $1\sigma$ region of the second component to the mixture model. (D) Location of MCMC realizations in disk $\alpha$ and $M_{tot}$, in green for $\{\alpha_1, M_{tot,1}\}$ and orange for $\{\alpha_2, M_{tot,2}\}$. (E) Marginalized posterior in $\alpha_1$ and $\alpha_2$. (F) Marginalized posterior in $f$, fraction of the mixture model in the first component. We have overplotted the distribution in $f$ for GK dwarfs from Figure 9, as well as the posterior from Ballard & Johnson (2014).

have studied how late-term dynamical instabilities can potentially reduce the number of planets in a system. The applicability of these results to the systems formed in our simulations is unclear because the initial structure of our planetary systems (e.g., planet masses and spacings) differs from theirs. We extended a subset of 32 simulations out to about 5 billion years. Of the simulations that we extended, the observed planet multiplicity distribution did not change significantly between 10 million and 5 billion years. It is possible that a larger sample would result in more dynamical instabilities but unlikely at a high enough rate to account for the number of singly transiting systems.

Tides are generally accepted to be an important factor in the orbital evolution of planets, particularly at small semimajor axes. Observations of exoplanets show an overall decrease in orbital eccentricity the closer the planet is to the star, which is attributed to tidal circularization. Tides would not have a large effect on our simulations because the timescale for tidal evolution is generally long compared to the duration of our simulations (Jackson et al. 2008). However, they would have a significant impact on the subsequent evolution of the orbits of the innermost planets in our simulations. In particular, the omission of tidal physics likely explains the increase in

eccentricity with decreasing semimajor axis seen in some of our simulations, which is not observed. The tidal circularization of orbits is also accompanied by an inward migration of order 0.01–0.05 au (Jackson et al. 2008). Both of these factors affect transit probability. Inward migration will increase the transit probability. However, orbital circularization will counteract this increase to some extent because eccentric orbits have a higher transit probability (Burke 2008).

### 5.4. Implications and Predictions

We note that the statistical comparisons made are not intended to ascertain the exact combination of initial conditions that must exist in planetesimal disks in order to produce the observed planetary systems. Rather, they are meant to emphasize the inability of models that assume all planetary systems have the same underlying architecture to reproduce the observations and, furthermore, to show that the range of system architectures that result from differing initial conditions in the planetesimal disk can reproduce important aspects of observations.

Nevertheless, we can draw some important conclusions from our analysis. To begin with, we, like other works (e.g., Hansen
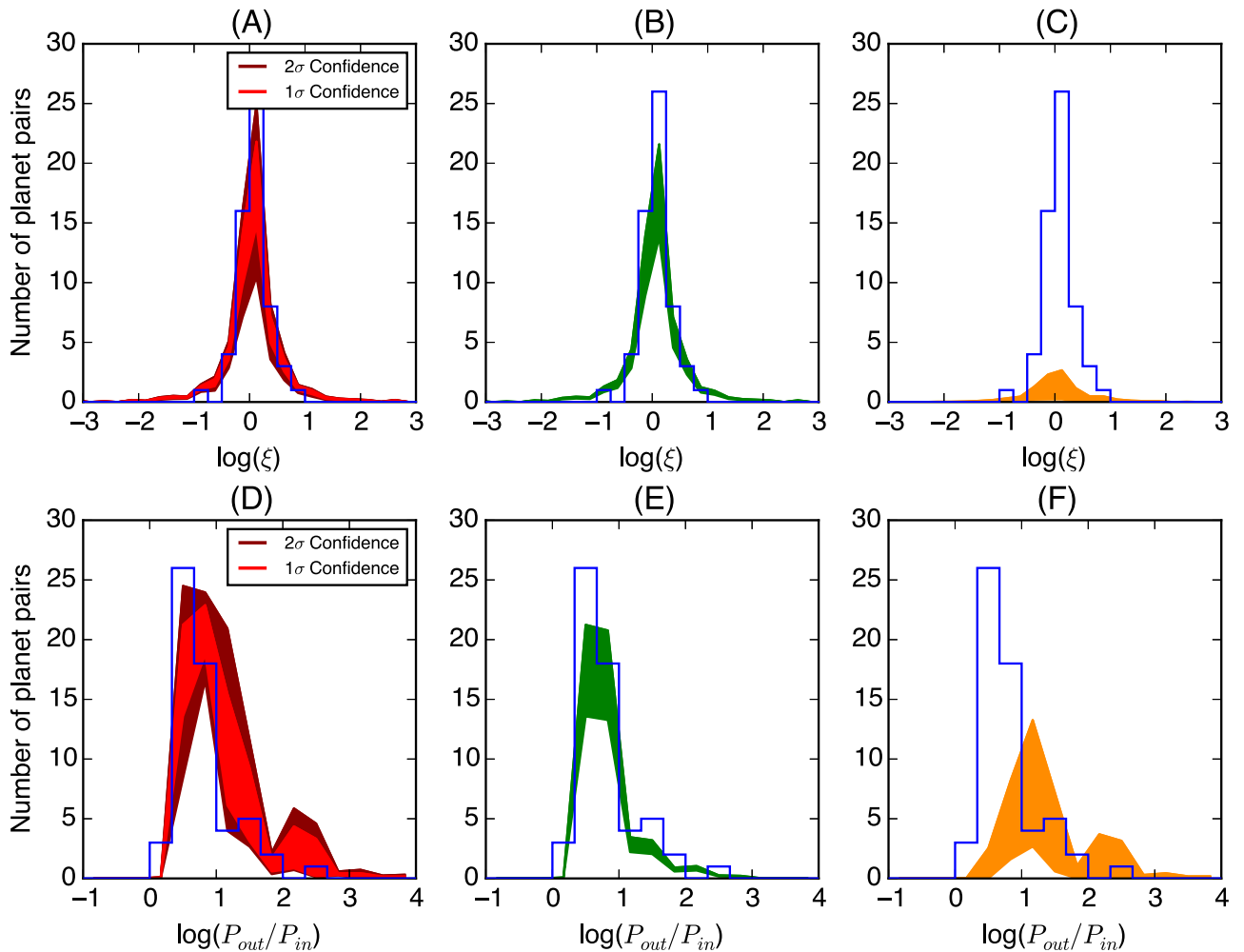
**Figure 14.** Predictions for period and duration ratio distributions, inferred from tranet fits for M dwarfs. Clockwise from top left: (A) Observed distribution of log of duration ratio, $\log(\xi)$, in blue. $1\sigma$ and $2\sigma$ confidence model regions are overplotted in light and dark red, respectively. (B) $1\sigma$ region of the first component to the mixture model. (C) $1\sigma$ region of the second component to the mixture model. (D) Observed distribution of $\log(P_{out}/P_{in})$ in blue, with $1\sigma$ and $2\sigma$ confidence model regions overplotted in light and dark red, respectively. (E) $1\sigma$ region of the first component to the mixture model. (F) $1\sigma$ region of the second component to the mixture model.

& Murray 2013), find that a model for the final assembly of close-in planets that relies solely on the gravitational interactions of the growing bodies without the need for additional physics (e.g., planet–disk interactions) can reproduce many of the observed characteristics of exoplanetary systems. Assuming that close-in planetary systems are predominantly gravitationally assembled in this way, we can say that some variation in the initial planetesimal disk structure is needed to form the variety of observed architectures (assuming there is no further relevant evolution of the systems after formation). In particular, some fraction of planetesimal disks must have initially steep radial surface density profiles while the rest have shallower surface density profiles.

The planetary systems that form from this range of initial conditions have significantly different final architectures. Because the systems that form from shallower surface density profiles typically only show at most one transiting planet and because these systems account for the majority of single-tranet systems, we can make some general testable predictions about single-tranet systems versus multiple-tranet systems:

1. Single-tranet systems contain fewer, more widely separated (in terms of mutual Hill radii) planets than do multiple-tranet systems. Although not directly observable, this may be inferred by the frequency and strength of transit timing variations.
2. Single-tranet systems should show larger stellar obliquity. This phenomenon is observed by both Morton & Winn (2014) and Li & Winn (2016).
3. Planet mass should increase with semimajor axis in single-tranet systems whereas in multiple-tranet systems it should decrease with semimajor axis.
4. Single-tranet systems should have higher average eccentricity. This prediction is borne out in part by Limbach & Turner (2015). They reported that average orbital eccentricity is a strong function of planetary multiplicity, with higher average eccentricity corresponding to fewer planets.

Additionally, because the diversity in architectures is determined at formation and is not the consequence of long-term evolution (e.g., dynamical instability), we predict that there should be no correlation in a system's multiplicity and its age.

In Figure 15, we show our predicted distribution in the Hill separation of *detected Kepler* planets that we infer from the
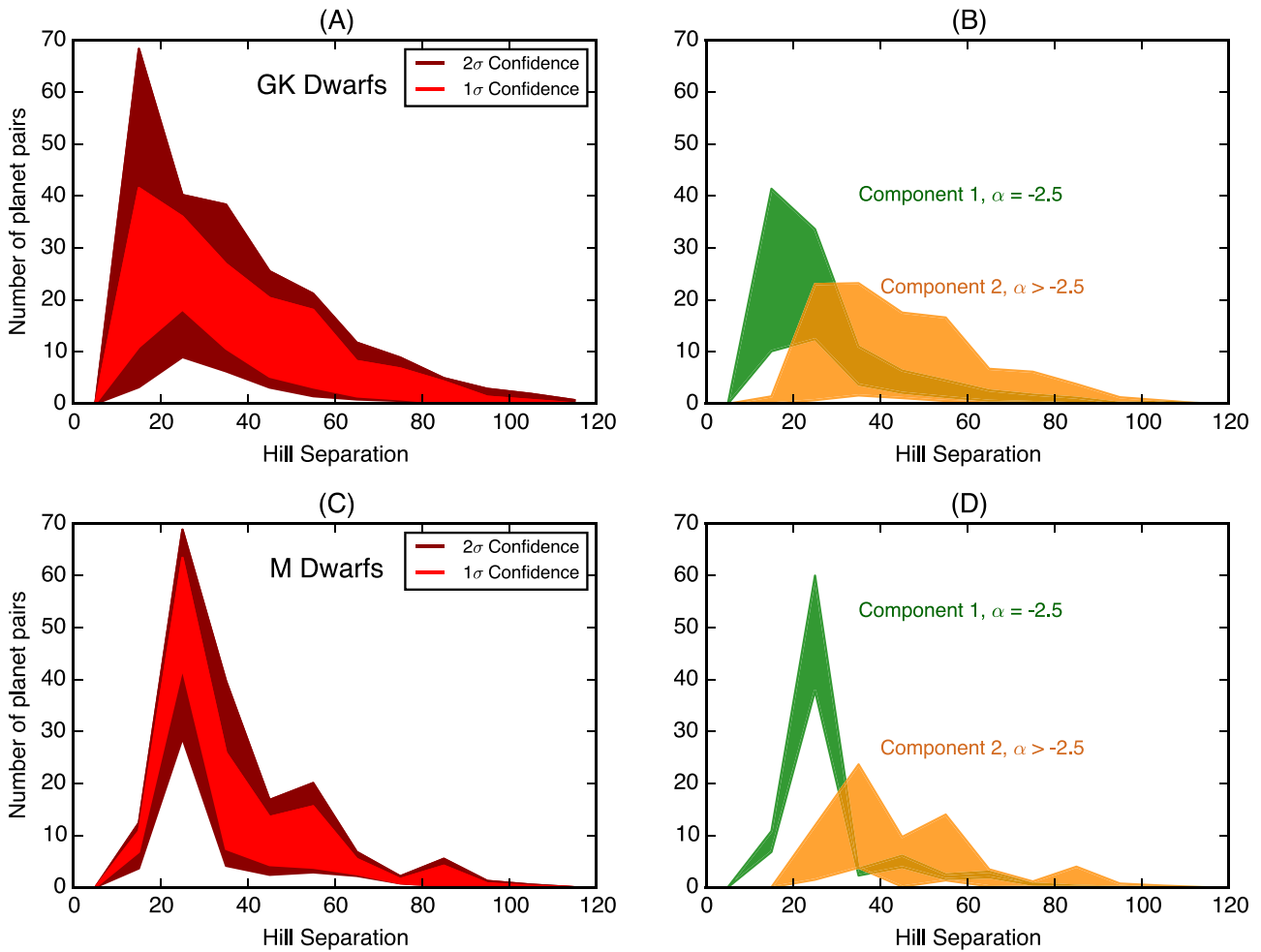
**Figure 15.** Predictions for mutual Hill separation distributions, inferred from tranet fits for GK dwarfs (top row) and M dwarfs (bottom row). Red curves, at right, depict the model prediction at 1σ and 2σ confidence in light and dark red, respectively. Contributions from each component of the mixture model at 1σ confidence indicated in orange (steeper surface density law) and green (shallower surface density power law).
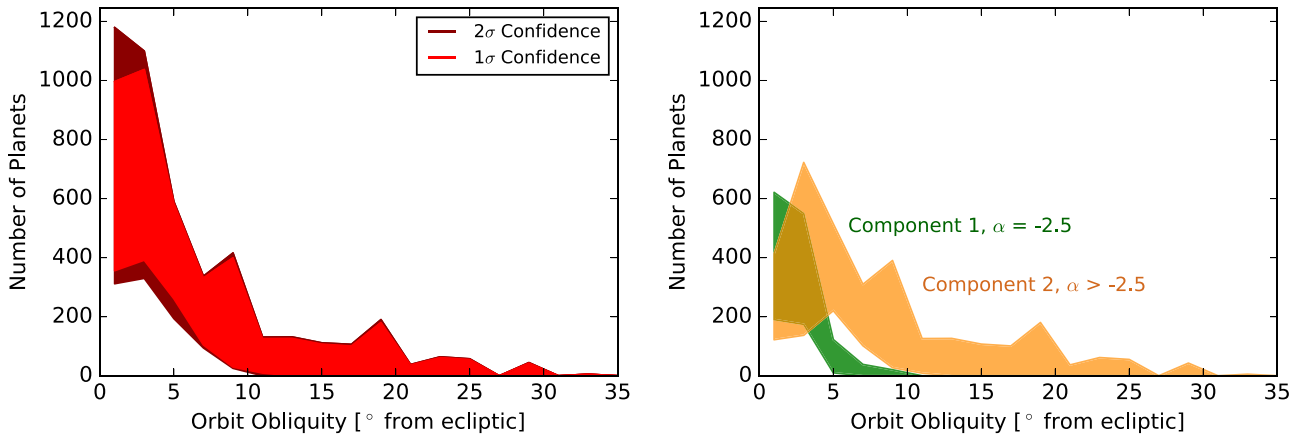


**Figure 16.** Predictions for spin–orbit obliquity for *Kepler* transiting planets orbiting GK dwarfs. Contributions from each component of the mixture model at 1σ confidence indicated in orange (steeper surface density law) and green (shallower surface density power law).

tranet comparison. The bulk of planet pairs have separations between ∼10 and 40 mutual Hill radii. Pu & Wu (2015) find that the distribution of separations for high multiplicity systems (4+) tends to be condensed into the 10–25 range, slightly smaller values than our overall distribution. However, the component of our distribution corresponding to the majority of multi-tranet systems and all high multiplicity systems

(α = −2.5) tends to produce planet pairs with smaller separations more consistent with the Pu & Wu (2015) distribution (see Figure 15(b)).

We show in Figure 16 the predicted stellar spin–orbit obliquities resulting from the same mixture model that reproduces the GK tranet sample. Predictably, the obliquities are lower within the flatter and dynamically cooler planetary

systems resulting from disks with steeper initial surface densities. We can compare this qualitatively to the results of Morton & Winn (2014), who found that systems with multiple tranets (likely to be drawn from this dynamically cooler population with inital $\alpha = -2.5$) have systematically lower obliquities than those with only one transiting planet (likelier to be drawn from the population with shallower initial $\alpha$). We observe the same general trend, but to a lesser extent. While Morton & Winn (2014) found that planets drawn from multiply transiting planetary systems possess obliquities of $10°$ on average, we predict more modest obliquities of a few degrees.

## 6. CONCLUSIONS

Recent analyses of exoplanet statistics have revealed that the configurations of planetary systems are not well described by a single-component model. Models that account for the frequency of multi-tranet systems significantly underpredict the number of single-tranet systems and models that can account for the number of single-tranet systems underpredict the number of multi-tranet systems. We have investigated the hypothesis that these differences in system architecture arise from variation in the primordial distribution of mass in planetesimal disks.

We performed a set of $N$-body simulations of late-stage planet formation, within which we varied initial planetesimal disk profiles. The resulting planetary systems are highly dependent on the initial conditions. Multiplicity, mutual inclinations, orbital separations, and eccentricities of planets vary significantly as a function of both total planetesimal disk mass and the radial distribution of this mass.

We compared our simulated systems to the *Kepler* yield of transiting planets. We apply the empirically determined *Kepler* completeness to our synthetic populations of planets. In this way, we compare the outcome of our simulations to the observed multiplicities from *Kepler*. We conclude, similarly to previous works, that we cannot replicate the *Kepler* yield of exoplanets with a single model for planet occurrence. Rather, the data favor a mixture model, with at least two sets of distinct initial conditions required to replicate the observations from *Kepler*. We find that the same mixture model that correctly predicts the tranet distribution from *Kepler* also self-consistently reproduces the period ratio and duration ratio distributions.

We find that the best-fit underlying population to our GK dwarf sample consists of one component accounting for approximately 20% of systems that forms from a very steep initial planetesimal disk. This component accounts for most of the multi-tranet systems. The other component (accounting for approximately 80% of systems) forms from planetesimal disks with shallower surface density profiles. Applying this analysis to M dwarfs, we see that the fraction of systems forming from steep planetesimal disk profiles increases to approximately 70%. We conclude that the differing nature of the *Kepler* dichotomy between GK and M dwarfs indicates that the process of planet formation varies with stellar mass.

## REFERENCES

Ballard, S., & Johnson, J. A. 2014, arXiv:1410.4192
Becker, J. C., & Adams, F. C. 2016, MNRAS, 455, 2980
Burke, C. J. 2008, ApJ, 679, 1566
Burke, C. J., Christiansen, J. L., Mullally, F., et al. 2015, ApJ, 809, 8
Chambers, J. E. 1999, MNRAS, 304, 793
Chiang, E., & Laughlin, G. 2013, MNRAS, 431, 3444
Christiansen, J. L., Clarke, B. D., Burke, C. J., et al. 2015, ApJ, 810, 95
Cossou, C., Raymond, S. N., Hersant, F., & Pierens, A. 2014, A&A, 569, A56
Dressing, C. D., & Charbonneau, D. 2015, ApJ, 807, 45
Fabrycky, D. C., Lissauer, J. J., Ragozzine, D., et al. 2014, ApJ, 790, 146
Fang, J., & Margot, J.-L. 2012, ApJ, 761, 92
Feroz, F., & Hobson, M. P. 2008, MNRAS, 384, 449
Feroz, F., Hobson, M. P., & Bridges, M. 2009, MNRAS, 398, 1601
Feroz, F., Hobson, M. P., Cameron, E., & Pettitt, A. N. 2013, arXiv:1306.2144
Figueira, P., Marmier, M., Boué, G., et al. 2012, A&A, 541, A139
Gaidos, E., & Mann, A. W. 2014, ApJ, 791, 54
Hansen, B. M. S., & Murray, N. 2012, ApJ, 751, 158
Hansen, B. M. S., & Murray, N. 2013, ApJ, 775, 53
Howard, A. W., Marcy, G. W., Bryson, S. T., et al. 2012, ApJS, 201, 15
Jackson, B., Barnes, R., & Greenberg, R. 2008, MNRAS, 391, 237
Johansen, A., Davies, M. B., Church, R. P., & Holmelin, V. 2012, ApJ, 758, 39
Johnson, E. T., Goodman, J., & Menou, K. 2006, ApJ, 647, 1413
Kokubo, E., & Ida, S. 2002, ApJ, 581, 666
Kretke, K. A., & Lin, D. N. C. 2012, ApJ, 755, 74
Laughlin, G., Steinacker, A., & Adams, F. C. 2004, ApJ, 608, 489
Li, G., & Winn, J. N. 2016, ApJ, 818, 5
Limbach, M. A., & Turner, E. L. 2015, PNAS, 112, 20
Lissauer, J. J., Ragozzine, D., Fabrycky, D. C., et al. 2011, ApJS, 197, 8
Masset, F. S., Morbidelli, A., Crida, A., & Ferreira, J. 2006, ApJ, 642, 478
McLachlan, G., & Peel, D. 2004, Finite Mixture Models (New York: Wiley)
Moriarty, J., & Fischer, D. 2015, ApJ, 809, 94
Morton, T. D., & Swift, J. 2014, ApJ, 791, 10
Morton, T. D., & Winn, J. N. 2014, ApJ, 796, 47
Mulders, G. D., Pascucci, I., & Apai, D. 2015, ApJ, 814, 130
Paardekooper, S. J., & Mellema, G. 2006, A&A, 459, L17
Petigura, E. A., Marcy, G. W., & Howard, A. W. 2013, ApJ, 770, 69
Pu, B., & Wu, Y. 2015, arXiv:150205449
Raymond, S. N., & Cossou, C. 2014, MNRAS, 440, L11
Silburt, A., Gaidos, E., & Wu, Y. 2015, ApJ, 799, 180
Swift, J. J., Johnson, J. A., Morton, T. D., et al. 2013, ApJ, 764, 105
Tanaka, H., Takeuchi, T., & Ward, W. R. 2002, ApJ, 565, 1257
Terquem, C., & Papaloizou, J. C. B. 2007, ApJ, 654, 1110
Terquem, C. E. J. M. L. J. 2003, MNRAS, 341, 1157
Volk, K., & Gladman, B. 2015, arXiv:150206558
Ward, W. 1997, Icar, 126, 261
Weidenschilling, S. J. 1977, Ap&SS, 51, 153
Wolfgang, A., Rogers, L. A., & Ford, E. B. 2015, arXiv:1504.07557
Wu, Y., & Lithwick, Y. 2011, ApJ, 735, 109
Xie, J.-W., Wu, Y., & Lithwick, Y. 2014, ApJ, 789, 165